Detection of Chemical Exchange in Methyl Groups of Macromolecules

Michelle L. Gill[1,2], Andrew Hsu[3], and Arthur G. Palmer, III[1]*

[1]Department of Biochemistry and Molecular Biophysics

Columbia University

630 West 168th Street

New York, NY 10032

[2]Current Address:

BenevolentAI

81 Prospect St, Brooklyn,

New York 11201

[3]Department of Chemistry

Columbia University

3000 Broadway

New York, NY 10027

*Voice: (212) 305-8675; email: agp6@columbia.edu

Abstract

The zero- and double-quantum methyl TROSY Hahn-echo and the methyl ^{1}H-^{1}H dipole-dipole cross-correlation nuclear magnetic resonance experiments enable estimation of multiple quantum chemical exchange broadening in methyl groups in proteins. The two relaxation rate constants are established to be linearly dependent using molecular dynamics simulations and empirical analysis of experimental data. This relationship allows chemical exchange broadening to be recognized as an increase in the Hahn-echo relaxation rate constant. The approach is illustrated by analyzing relaxation data collected at three temperatures for *E. coli* ribonclease HI and by analyzing relaxation data collected for different cofactor and substrate complexes of *E. coli* AlkB.

Keywords: AlkB; cross-correlated relaxation; double-quantum relaxation; dynamics; multiple-quantum relaxation; ribonuclease HI; zero-quantum relaxation

Highlights

- Method for detecting chemical exchange in methyl groups of biological macromolecules.
- Chemical exchange detected in key substrate-binding loop of the enzyme ribonuclease HI.
- Confirmation of chemical exchange contributions in the enzyme AlkB.

Introduction

An important first step in characterizing micro-to-millisecond time scale dynamic processes in proteins and other biological macromolecules consists of identifying which sites are subject to significant chemical exchange broadening in NMR spectroscopic experiments [1]. A very general approach relies on the scaling of chemical exchange broadening with the magnitude of the static magnetic field [2-4]. Other approaches rely on high-power spin-locking radiofrequency fields to suppress chemical exchange broadening for comparison with a reference experiment in which exchange is minimally suppressed [5-7]. For backbone ^{15}N spins in U-^{2}H, U-^{15}N} proteins, the TROSY Hahn-echo experiment is very efficient [8]. In this experiment, the exchange-free relaxation rate constant is estimated as $R_2^0 = \kappa\eta_{xy}$ in which η_{xy} is the transverse ^{1}H-^{15}N dipole/^{15}N CSA transverse relaxation interference rate constant, which depends on physical parameters and can be calculated *a priori*, or more often measured empirically, for a subset of spins not subject to exchange [9,10].

Relaxation of ^{1}H and ^{13}C spins in methyl groups is a powerful probe of side-chain conformational dynamics, and experimental methods for measurement of single- and multiple-quantum relaxation rate constants have been developed extensively by Kay and coworkers [11-19]. We described zero- and double-quantum methyl TROSY Hahn-echo experiments [20] and subsequently used these experiments in an investigation of the role of conformational dynamics in gating activity of the *E. coli* DNA repair enzyme AlkB [21]. The Hahn-echo experiment minimally suppresses chemical exchange effects; consequently, exchange can be detected by comparison with a second experiment that either suppresses chemical exchange [22] or that is independent of chemical exchange [23]. Herein, the methyl ^{1}H-^{1}H dipole-dipole cross-correlation experiment developed by Tugarinov and Kay [19] serves as the exchange-free reference experiment. The combination of methyl TROSY Hahn-echo and methyl ^{1}H-^{1}H dipole-dipole

cross-correlation experiments allows facile identification of chemical exchange in methyl groups [23]. The approach is illustrated for both *E. coli* ribonuclease HI (RNase H) and AlkB.

The expression for differential relaxation of zero- and double-quantum coherence (ΔR_{MQ}) measured in the Hahn-echo experiments is:

$$\Delta R_{MQ} = (R_{DQ} - R_{ZQ})/2 = \Delta R^0 + \Delta R_{ex}/2 \tag{1}$$

in which [14,20,24,25]:

$$\begin{aligned}\Delta R^0 &= \frac{2}{5}\left(\frac{\mu_0}{4\pi}\right)^2 \hbar^2 \tau_c \gamma_C \gamma_H^3 \left\{\frac{8\gamma_D^2}{3\gamma_H^2}\sum_{D^E}\left\langle \frac{P_2(\cos\theta_{CD^E H})}{(r_{CD^E} r_{HD^E})^3}\right\rangle + \sum_{H^E}\left\langle \frac{P_2(\cos\theta_{CH^E H})}{(r_{CH^E} r_{HH^E})^3}\right\rangle\right\} \\ &= \frac{2}{5}\left(\frac{\mu_0}{4\pi}\right)^2 \hbar^2 \tau_c \gamma_C \gamma_H^3 \Gamma\end{aligned} \tag{2}$$

$$\Delta R_{ex} = 4 p_1 p_2 \Delta\omega_C \Delta\omega_H / k_{ex} \tag{3}$$

μ_0 is the vacuum permeability, $\hbar$ is Planck's constant divided by 2π, τ_c is the effective overall rotational correlation time of the macromolecule, γ_X is the magnetogyric ratio (X= C, D, and H to represent ^{13}C, ^{2}H, and ^{1}H, respectively), r_{CD^E} and r_{HD^E} are the distances from the methyl ^{13}C and ^{1}H to remote ^{2}H spins in the molecule, r_{CH^E} and r_{HH^E} are the distances from the methyl ^{13}C and ^{1}H to remote ^{1}H spins in the protein, $P_2(x) = (3x^2 - 1)/2$ is the second Legendre polynomial, and θ_{CXH} is the angle between the C-X-H atoms. The term in brackets has been denoted Γ for convenience. The first summation is over all the remote ^{2}H spins and the second summation is over all the remote ^{1}H spins in the molecule; the relative size of these two summations depends upon the pattern and extent of deuteration of the protein and the fractional content of D_2O in the sample buffer (*vide infra*). Angle brackets indicate ensemble averaging to account for fast molecular dynamics. Rotation of the methyl group was treated by averaging distances for the

three methyl H-atom positions. The expression for ΔR_{ex} is the fast-limit expression for two-site exchange for convenience; in this expression, p_1 and p_2 are the populations of the two states of the molecule, $\Delta\omega_C$ and $\Delta\omega_H$ are the differences in ^{13}C and ^{1}H chemical shifts for a spin in the two states, $k_{ex} = k_1 + k_{-1}$, and k_1 and k_{-1} are the forward and reverse reaction rate constants. Expressions for ΔR_{ex} for other time scales have been given in the literature [26]. The ^{1}H-^{1}H dipole-dipole cross-correlated relaxation rate constant for pairs of ^{1}H spins in a methyl group is given by [19]:

$$\eta_{HH} = \frac{9}{10}\left(\frac{\mu_0}{4\pi}\right)^2 \hbar^2 \gamma_H^4 P_2(\cos\theta_{HH})^2 S^2_{axis} \tau_c \left\langle r_{HH}^{-6} \right\rangle \tag{4}$$

in which $\theta_{HH} = \pi/2$ is the angle between a vector of length r_{HH} between two ^{1}H spins in the methyl group and the methyl symmetry axis, and S^2_{axis} is the generalized order parameter for a unit vector along the symmetry axis of the methyl group. Importantly, this rate constant is independent of any exchange contributions.

Experimental data reported below for RNase H suggest a linear correlation exists between ΔR^0 and η_{HH} and hence between Γ and S^2_{axis}:

$$\Gamma = \alpha S^2_{axis} + \beta \tag{5}$$

This correlation also is supported by molecular dynamics (MD) simulations (*vide infra*) and reflects the dependence of both Γ and S^2_{axis} on packing density [27-29] Combining Eqs. 2, 4, and 5 yields:

$$\begin{aligned} \Delta R^0 &= \frac{4}{9} P_2(\cos\theta_{HH})^{-2} \left\langle r_{HH}^{-6} \right\rangle^{-1} \gamma_C \gamma_H^{-1} \alpha \eta_{HH} + \frac{2}{5}\left(\frac{\mu_0}{4\pi}\right)^2 \hbar^2 \tau_c \gamma_C \gamma_H^3 \beta \\ &= \kappa \eta_{HH} + \varepsilon \end{aligned} \tag{6}$$

The values of α and β, or κ and ε, can be estimated from MD simulations, or by examining the distribution of experimental values of ΔR_{MQ} relative to η_{HH}, because contributions from ΔR_{ex} will only increase ΔR_{MQ}. Combining Eqs. 1 and 6 yields $\Delta R_{ex} = 2(\Delta R_{MQ} - \kappa\eta_{HH} - \varepsilon)$ as the key result for detection of chemical exchange contributions to multiple quantum relaxation in methyl spin systems.

Methods

Molecular dynamics simulations. A full description of the MD simulations and comparison with NMR spin relaxation data for RNase H will be published elsewhere. Briefly, the system was prepared and simulations were performed using the Schrödinger Maestro Protein Preparation Wizard version 11.3.016 [30,31], Schrödinger Multisim version 3.8.5.19 [30], and Desmond version 5.5 [31]. Hydrogen atoms were added to the x-ray crystal structure (PDB code 2RN2, 1.5 Å resolution) consistent with pH = 5.5 to mimic the conditions used in NMR experiments; solvated with TIP3P water in an orthorhombic box with a 10Å buffer region from solute to box boundary [32]; and neutralized with Cl^- ions. The system was relaxed and energy-minimized prior to a 5 ns constant pressure and constant temperature (NPT) equilibration simulation. Twenty structures were extracted from the trajectory (structures were chosen roughly every 250 ps with the proviso that the box volume was close to the average box volume over the 5 ns of the simulation). These structures were ranked based on their MolProbity score [33,34] and the top two structures were chosen as the starting structures for two independent 1-μs constant volume and constant temperature (NVT) simulations. Volume and temperature reached equilibrium values in less than 100 ps in all simulations. A RESPA integrator was used with a time step of 1 fs for bonded and short-range non-bonded interactions, and 3 fs for long-range electrostatics [35]. Electrostatics were calculated with the particle mesh Ewald method using a 9 Å cutoff [36-38]. Simulations were performed at 300 K using a Nosé-Hoover thermostat [39,40].

Additionally, the NPT ensemble used a Martyna-Tobias-Klein (MTK) barostat [41]. Coordinate sets were saved every 10 ps for NPT simulations and 4.5 ps for NVT simulations.

NMR spectroscopy. $^{13}C^{\epsilon}$-methionine AlkB was expressed and purified and the NMR spin relaxation parameters were determined at 21.1 T as previously described [21]. The expression and purification of U-^{2}H and [^{13}C $^{1}H_3$] Ile δ1 and stereospecifically labeled Val γ and Leu δ RNase H has also been described [20]. For RNase H, all NMR experiments were performed on a Bruker Avance spectrometer with a triple resonance *z*-axis gradient cryoprobe and operating at 14.1 T. Each experiment was performed at 283, 300, and 310 K, and the Hahn echo data collected at 283 K have been previously reported [20]. Temperature was calibrated using 98% $^{2}H_4$-methanol [42]. The zero- and double-quantum Hahn echo data collected at 300 and 310 K used 1024 × 188 ($t_2 \times t_1$) complex points, 4.5 × 7.2 kHz spectral widths, and relaxation delays of $n/(2J_{CH})$ where J_{CH} = 128 Hz and n = {1, 25, 40} for 300 K and n = {1, 10, 25, 35, 40, 45} for 310 K. The ^{1}H-^{1}H cross correlated relaxation data were collected with 1024 × 256 complex points, 4.9 × 7.3 kHz spectral widths, and relaxation delays of 2, 8, 20, 40, and 50 ms at each of the three temperatures. Data were processed with NMRPipe [43] using a cosine bell function for apodization in the indirect dimension. Assignments were made using Sparky [44]. Peak intensities for the Hahn Echo data acquired at 283 K were determined from ten iterative rounds of peak fitting performed in NMRPipe, as described previously [20]. The remaining peak intensities were determined using Sparky. Further data analysis and visualization of results were performed using Python [45-51].

Results and Discussion

The bracketed term denoted Γ in Eq. 2 must be calculated from MD simulations or estimated empirically. In the present work, this term was calculated for Ile δ1, Leu δ1 and δ2, and Val γ1 and γ2 methyl groups in RNase H as the average value from two 1-μs MD simulations. The calculations included the 25 (out of 46) methyl groups for which the absolute

differences between simulated and experimental values of S^2_{axis} were less than 0.1; however, results were not substantially altered by changing the maximum difference to 0.05 or 0.15. The experimental values of S^2_{axis} are described elsewhere[52] and compared to simulated values in Figure 1a. The graph of Γ versus the simulated value of S^2_{axis} is shown in Figure 1b. The calculated points cluster into two subsets with different slopes. The slopes were determined using the non-parametric Thiel-Sen estimator. The intercepts for both sets of data were set to the intercept determined for the subset of data with the smaller slope. The fitted values of α gave low and high estimates of $\kappa_{ILV} = 0.030$ and 0.080, respectively. The fitted value of β gave $\varepsilon_{ILV} = 0.37\ s^{-1}$.

The calculations were validated by calculating ΔR^0 from Eq. 1 for the same 25 methyl groups used for Figure 1 and comparing to the mean values of ΔR_{MQ} for protein L and malate synthase G reported by Kay and coworkers [14]. A graph of the experimental and predicted results is shown in Figure 2. The predicted slope differs from the fitted slope by ~10%, well within the spread of experimental values, and the standard deviation of the predicted slope is in good agreement with the experimental standard deviations shown in the figure. For the highly deuterated RNase H sample, the predicted relaxation contribution from remote ^{2}H spins (the first sum in Eq. 2) is ~10-fold larger than from remote ^{1}H spins (the second sum in Eq. 2).

The values of ΔR_{MQ} and η_{HH} for Ile δ1, Leu δ1 and δ2, and Val γ1 and γ2 methyl groups in RNase H at 283, 300, and 310 K are shown in Figure 3. Graphs of ΔR_{MQ} versus η_{HH} are shown in Figure 4. Lines plotted using the calculated values of κ_{ILV} and ε_{ILV} are shown. The differences between the lines shown for the two estimates of κ_{ILV} set a lower bound on the smallest exchange contribution that can be detected by this method. Note that ΔR_{ex}, and hence ΔR_{MQ}, can be negative depending on the relative signs of $\Delta\omega_C$ and $\Delta\omega_H$, as shown by Eq. 3. Larger values of $|\Delta R_{MQ}|$ for Val 98 γ1, Val 101 γ1, and Leu 103 δ1 are consistent with significant conformational

exchange; elevated values of $|\Delta R_{MQ}|$ also are observed for Ile 78 δ1 and Ile 82 δ1 at 283 K. Excluding these residues, a linear fit to ΔR_{MQ} versus η_{HH} using the 'leiv' Bayesian algorithm in the statistics program R gave $\kappa_{ILV} = 0.094 \pm 0.003$ and $\varepsilon_{ILV} = 0.01 \pm 0.03$, in good agreement with the larger of the two values of κ_{ILV} obtained from the MD simulations.

The resonances of Val 98 γ1, Val 101 γ1, and Leu 103 δ1 are notably broadened, beyond that of the other residues in RNase H. Graphs of ΔR_{ex} versus $1/T$ for these residues are shown in Figure 4d. For fast-limit two-site exchange with site populations $p_1 >> p_2$, the apparent activation energy is [53]:

$$E_{app}^{\dagger} = E_1^{\dagger} + \Delta E(1-3p_1^0) = \bar{E}^{\dagger} - \Delta E(p_1^0 - p_2^0) \qquad (7)$$

in which $E_1^{\dagger}$, and $E_{-1}^{\dagger}$ are the activation barriers in the forward and reverse reaction directions, $\Delta E = E_1^{\dagger} - E_{-1}^{\dagger}$, $p_1{}^0$ and $p_2{}^0$ are the site populations at a reference temperature T^0, and $\bar{E}^{\dagger} = p_2^0 E_1^{\dagger} + p_1^0 E_{-1}^{\dagger}$ is the apparent activation energy that would be obtained from $d\ln(k_{ex})/d(1/T)$ rather than $d\ln(\Delta R_{ex})/d(1/T)$. Consequently, $E_{app}^{\dagger}$ underestimates $\bar{E}^{\dagger}$ by $\Delta E(p_1^0 - p_2^0) \approx \Delta E$. Values of $E_{app}^{\dagger}$ are given in Table 1 for Val 98 γ1, Val 101 γ1, and Leu103 δ1. Values of the activation barriers are consistent with results from $R_{1\rho}$ measurements for backbone ^{15}N spins [54]. Each of these residues has been demonstrated to be directly involved in or located within the substrate-binding handle region associated with conformational transitions from open to closed states by ^{15}N amide spin relaxation experiments and/or molecular dynamics simulations [54-56].

Figure 5 shows a graph of ΔR_{MQ} versus η_{HH} based on data previously reported (see Figure 5C&D in Ergel, *et. al* [21]) for the DNA repair enzyme AlkB in complex with Zn^{2+}; Zn^{2+} and the co-substrate 2-oxoglutarate (2OG); and Zn^{2+}, 2OG, and DNA substrate 5′-CAmAAT-3′. Results are shown for the four Met residues in AlkB: Met 49, Met 57, and Met 61 are located in the active site or nucleotide recognition lid (NRL) and Met 92 is located at a hinge between the

core domain and the NRL. A number of residues in the various complexes exhibit conformational exchange broadening, with the largest ΔR_{ex} observed for M49 in the 2OG complex. Notably, the NMR spectra of the methyl groups of Met 49, Met 57 and Met 61 in the ternary complex show sharp resonance signals[21], suggesting that exchange is absent for the active site residues in this complex. As shown above for RNase H, ε has a small effect on the analysis; accordingly, ε_{Met} was set to zero and the weighted-mean ratio $\Delta R_{MQ}/\eta_{HH} = 0.093 \pm 0.009$ for Met 49, Met 57 and Met 61 was set to κ_{Met}. These results are consistent with exchange between an open and closed conformer in the Zn and Zn/2OG enzyme complexes, and with significant line broadening of M49 in the 2OG complex due to nearly equal populations of open and closed conformations in the Zn/2OG complex and a relatively large chemical shift difference between the two states ($\Delta\omega_C >= 2.1$ ppm) for this residue [21,57,58].

Conclusion

The combination of the zero- and double-quantum methyl TROSY Hahn-echo experiment [20] and the methyl ^{1}H-^{1}H dipole-dipole cross-correlation experiment [19] provide a convenient experimental approach to determining $\Delta R_{ex} = 2(\Delta R_{MQ} - \kappa\eta_{HH} - \varepsilon)$ in a fashion that is analogous to the ^{1}H-^{15}N TROSY Hahn-echo experiment. The proportionality constant κ can be calculated accurately from MD simulations or from empirical comparisons between ΔR_{MQ} and η_{HH} and depends on the labeling strategy employed; the intercept ε is small in the examples considered herein. Application of this approach to relaxation data collected at three temperatures identifies residues Val 98, Val 101, and Leu 103 as key probes of conformational dynamics of the substrate binding handle region of RNase H. A second application of this approach confirms previous observations that chemical exchange broadening reflects an open-closed equilibrium of nucleotide recognition lid of AlkB. These applications suggest that the proposed approach has

wide application in studies of the conformational dynamics of proteins and other biological macromolecules [23].

Acknowledgments

Support from National Institutes of Health grants GM089047 (M.L.G.), GM008281 (A. H.). and GM050291 (A.G.P.) is acknowledged gratefully. The AVANCE 600 NMR spectrometer at Columbia University was purchased with the support of NIH grant RR026540. Some of the work presented here was conducted at the Center on Macromolecular Dynamics by NMR Spectroscopy located at the New York Structural Biology Center, supported by a grant from the NIH National Institute of General Medical Sciences (P41 GM118302). A.G.P. is a member of the New York Structural Biology Center. A preliminary account of this work was presented as poster 96 at the 56th Experimental NMR Conference (2016). We thank Richard Friesner (Columbia University) and Martha Beckwith (Advanced Science Research Center, City University of New York) for helpful discussions and Richard Friesner for access to computational facilities.

References

1. Palmer, A.G. & Koss, H. Chemical exchange. *Meth. Enzymol.* **615**, 177-236 (2019).
2. Phan, I.Q.H., Boyd, J. & Campbell, I.D. Dynamic studies of a fibronectin type I module pair at three frequencies: Anisotropic modelling and direct determination of conformational exchange. *J. Biomol. NMR* **8**, 369-378 (1996).
3. O'Connell, N.E., Grey, M.J., Tang, Y., Kosuri, P., Miloushev, V.Z., Raleigh, D.P. & Palmer, A.G. Partially folded equilibrium intermediate of the villin headpiece HP67 defined by ^{13}C relaxation dispersion. *J. Biomol. NMR* **45**, 85-98 (2009).
4. Millet, O. & Palmer, A.G. The static magnetic field dependence of chemical exchange linebroadening defines the chemical shift time scale. *J. Am. Chem. Soc.* **122**, 2867-2877 (2000).
5. Ban, D., Mazur, A., Carneiro, M.G., Sabo, T.M., Giller, K., Koharudin, L.M., Becker, S., Gronenborn, A.M., Griesinger, C. & Lee, D. Enhanced accuracy of kinetic information from CT-CPMG experiments by transverse rotating-frame spectroscopy. *J. Biomol. NMR* **57**, 73-82 (2013).
6. Reddy, J.G., Pratihar, S., Ban, D., Frischkorn, S., Becker, S., Griesinger, C. & Lee, D. Simultaneous determination of fast and slow dynamics in molecules using extreme CPMG relaxation dispersion experiments. *J. Biomol. NMR* **70**, 1-9 (2018).
7. Hansen, D.F., Feng, H., Zhou, Z., Bai, Y. & Kay, L.E. Selective characterization of microsecond motions in proteins by NMR relaxation. *J. Am. Chem. Soc.* **131**, 16257-65 (2009).
8. Wang, C. & Palmer, A.G. Solution NMR methods for quantitative identification of chemical exchange in ^{15}N-labeled proteins. *Magn. Reson. Chem.* **41**, 866-876 (2003).
9. Kroenke, C.D., Loria, J.P., Lee, L.K., Rance, M. & Palmer, A.G. Longitudinal and transverse ^{1}H-^{15}N dipolar/^{15}N chemical shift anisotropy relaxation interference: unamiguous

determination of rotational diffusion tensors and chemical exchange effects in biological macromolecules. *J. Am. Chem. Soc.* **120**, 7905-7915 (1998).

10. Fushman, D. & Cowburn, D. Model-independent analysis of ^{15}N chemical shift anisotropy from NMR relaxation data. Ubiquitin as a test example. *J. Am. Chem. Soc.* **120**, 7109-7110 (1998).
11. Tugarinov, V., Hwang, P.M., Ollerenshaw, J.E. & Kay, L.E. Cross-correlated relaxation enhanced ^{1}H-^{13}C NMR spectroscopy of methyl groups in very high molecular weight proteins and protein complexes. *J. Am. Chem. Soc.* **125**, 10420-8 (2003).
12. Korzhnev, D.M., Kloiber, K., Kanelis, V., Tugarinov, V. & Kay, L.E. Probing slow dynamics in high molecular weight proteins by methyl-TROSY NMR spectroscopy: Application to a 723-residue enzyme. *J. Am. Chem. Soc.* **126**, 3964-3973 (2004).
13. Korzhnev, D.M., Kloiber, K. & Kay, L.E. Multiple-quantum relaxation dispersion NMR spectroscopy probing millisecond time-scale dynamics in proteins: theory and application. *J. Am. Chem. Soc.* **126**, 7320-9 (2004).
14. Tugarinov, V., Sprangers, R. & Kay, L.E. Line narrowing in methyl-TROSY using zero-quantum ^{1}H-^{13}C NMR spectroscopy. *J. Am. Chem. Soc.* **126**, 4921-5 (2004).
15. Tugarinov, V., Kay, L.E., Ibraghimov, I. & Orekhov, V.Y. High-resolution four-dimensional ^{1}H-^{13}C NOE spectroscopy using methyl-TROSY, sparse data acquisition, and multidimensional decomposition. *J. Am. Chem. Soc.* **127**, 2767-75 (2005).
16. Tugarinov, V., Ollerenshaw, J.E. & Kay, L.E. Dipolar dynamic frequency shifts in multiple-quantum spectra of methyl groups in proteins: correlation with side-chain motion. *Magn. Reson. Chem.* **44**, S122-9 (2006).
17. Tugarinov, V. & Kay, L.E. Relaxation rates of degenerate ^{1}H transitions in methyl groups of poteins as reporters of side-chain dynamics. *J. Am. Chem. Soc.* **128**, 7299-7308 (2006).

18. Tugarinov, V. & Kay, L.E. Separating degenerate ^{1}H transitions in methyl group probes for single-quantum ^{1}H-CPMG relaxation dispersion NMR spectroscopy. *J. Am. Chem. Soc.* **129**, 9514-21 (2007).

19. Tugarinov, V., Sprangers, R. & Kay, L.E. Probing side-chain dynamics in the proteasome by relaxation violated coherence transfer NMR spectroscopy. *J. Am. Chem. Soc.* **129**, 1743-1750 (2007).

20. Gill, M.L. & Palmer, A.G. Multiplet-filtered and gradient-selected zero-quantum TROSY experiments for $^{13}C^{1}H_{3}$ methyl groups in proteins. *J. Biomol. NMR* **51**, 245-51 (2011).

21. Ergel, B., Gill, M.L., Brown, L., Yu, B., Palmer, A.G. & Hunt, J.F. Protein dynamics control the progression and efficiency of the catalytic reaction cycle of the Escherichia coli DNA-repair enzyme AlkB. *J. Biol. Chem.* **289**, 29584-601 (2014).

22. Toyama, Y., Osawa, M., Yokogawa, M. & Shimada, I. NMR method for characterizing microsecond-to-millisecond chemical exchanges utilizing differential multiple-quantum relaxation in high molecular weight proteins. *J. Am. Chem. Soc.* **138**, 2302-2311 (2016).

23. Toyama, Y., Kano, H., Mase, Y., Yokogawa, M., Osawa, M. & Shimada, I. Dynamic regulation of GDP binding to G proteins revealed by magnetic field-dependent NMR relaxation analyses. *Nat. Commun.* **8**, 14523 (2017).

24. Konrat, R. & Sterk, H. Cross-correlation effects in the transverse relaxation of multiple-quantum transitions of heternuclear spin systems. *Chem. Phys. Lett.* **203**, 75-80 (1993).

25. Norwood, T.J., Tillett, M.L. & Lian, L.-Y. Influence of cross-correlation between the chemical shift anisotropies of pairs of nuclei on multiple-quantum relaxation rates in macromolecules. *Chem. Phys. Lett.* **300**, 429-434 (1999).

26. Wang, C. & Palmer, A.G. Differential multiple quantum relaxation caused by chemical exchange outside the fast exchange limit. *J. Biomol. NMR* **24**, 263-268 (2002).

27. Trott, O., Siggers, K., Rost, B. & Palmer, A.G. Protein conformational flexibility prediction using machine learning. *J. Magn. Reson.* **192**, 37-47 (2008).

28. Zhang, F. & Brüschweiler, R. Contact model for the prediction of NMR N-H order parameters in globular proteins. *J. Am. Chem. Soc.* **124**, 12654-12655 (2002).

29. Ming, D. & Brüschweiler, R. Prediction of methyl-side chain dynamics in proteins. *J. Biomol. NMR* **29**, 363-368 (2004).

30. Banks, J.L., Beard, H.S., Cao, Y., Cho, A.E., Damm, W., Farid, R., Felts, A.K., Halgren, T.A., Mainz, D.T., Maple, J.R., Murphy, R., Philipp, D.M., Repasky, M.P., Zhang, L.Y., Berne, B.J., Friesner, R.A., Gallicchio, E. & Levy, R.M. Integrated Modeling Program, Applied Chemical Theory (IMPACT). *J. Comput. Chem,* **26**, 1752-1780 (2005).

31. Sastry, G.M., Adzhigirey, M., T, D., Annabhimoju, R. & Sherman, W. Protein and ligand preparation: parameters, protocols, and influence on virtual screening enrichments. *J. Comput. Aided Mol. Des.* **27**, 221-234 (2013).

32. Jorgensen, W.L., Chandrasekhar, J., Madura, J.D., Impey, R.W. & Klein, M.L. Comparison of simple potential functions for simulating liquid water. *J. Chem. Phys.* **79**, 926-935 (1983).

33. Chen, V.B., Arendall 3rd, W.B., Headd, J.J., Keedy, D.A., Immormino, R.M., Kapral, G.J., Murray, L.W., Richardson, J.S. & Richardson, D.C. MolProbity: all-atom structure validation for macromolecular crystallography. *Acta Crystallogr. D Biol. Crystallogr.* **66**, 12-21 (2010).

34. Williams, C.J., Headd, J.J., Moriarty, N.W., Prisant, M.G., Videau, L.L., Deis, L.N., Verma, V., Keedy, D.A., Hintze, B.J., Chen, V.B., Jain, S., Lewis, S.M., Arendall, W.B., Snoeyink, J., Adams, P.D., Lovell, S.C., Richardson, J.S. & Richardson, D.C. MolProbity: More and better reference data for improved all‐atom structure validation. *Protein Sci.* **27**, 293-315 (2018).

35. Tuckerman, M., Berne, B.J. & Martyna, G.J. Reversible multiple time scale molecular dynamics. *J. Chem. Phys.* **97**, 1990-2001 (1992).

36. Cheatham, T.E., III, Miller, J.L., Fox, T., Darden, T.A. & Kollman, P.A. Molecular dynamics simulations on solvated biomolecular systems: The particle mesh Ewald method leads to stable trajectories of DNA, RNA, and proteins. *J. Am. Chem. Soc.* **117**, 4193-4194 (1995).

37. Darden, T., York, D. & Pedersen, L. Particle mesh Ewald: An N · log(N) method for Ewald sums in large systems. *J. Chem. Phys.* **98**, 10089-10092 (1993).

38. York, D.M., Darden, T.A. & Pedersen, L.G. The effect of long-range electrostatic interactions in simulations of macromolecular crystals: A comparison of the Ewald and truncated list methods. *J. Chem. Phys.* **99**, 8345-8348 (1993).

39. Nosé, S. A unified formulation of the constant temperature molecular dynamics methods. *J. Chem. Phys.* **81**, 511-519 (1984).

40. Hoover, W.G. Canonical dynamics: Equilibrium phase-space distributions. *Phys, Rev. A* **31**, 1695-1697 (1985).

41. Martyna, G.J., Tobias, D.J. & Klein, M.L. Constant pressure molecular dynamics algorithms. *J. Chem. Phys.* **101**, 4177-4189 (1994).

42. Findeisen, M., Brand, T. & Berger, S. A ^{1}H-NMR thermometer suitable for cryoprobes. *Magn. Reson. Chem.* **45**, 175-178 (2007).

43. Delaglio, F., Grzesiek, S., Vuister, G.W., Zhu, G., Pfeifer, J. & Bax, A. NMRPipe: a multidimensional spectral processing system based on UNIX pipes. *J. Biomol. NMR* **6**, 277-293 (1995).

44. Goddard, T. & Kneller, D.G. SPARKY 3. (University of California, San Francisco).

45. Helmus, J.J. & Jaroniec, C.P. NMRglue: an open source Python package for the analysis of multidimensional NMR data. *J. Biomol. NMR* **55**, 355-367 (2013).

46. McKinney, W. Data structures for statistical computing in Python. in *Proceedings of the 9th Python in Science Conference* (eds van der Walt, S. & Millman, J.) 51-56 (2010).

47. Millman, K.J. & Aivazis, M. Python for scientists and engineers. *IEEE Comput. Sci. Eng.* **13**, 9-12 (2011).

48. Oliphant, T.E. Python for scientific computing. *IEEE Comput. Sci. Eng.* **9**, 10-20 (2007).

49. Pérez, F. & Granger, B.E. IPython: A system for interactive scientific computing. *IEEE Comput. Sci. Eng.* **9**, 21-29 (2007).

50. van der Walt, S., Colbert, S.C. & Varoquaux, G. The NumPy array: A structure for efficient numerical computation. *IEEE Comput. Sci. Eng.* **13**, 22-30 (2011).

51. Hunter, J.D. Matplotlib: A 2D graphics environment. *IEEE Comput. Sci. Eng.* **9**, 90-95 (2007).

52. Hsu, A., O' Brien, P.A., Bhattacharya, S., Rance, M. & Palmer, A.G. Enhanced spectral density mapping through combined multiple-field deuterium $^{13}CH_2D$ methyl spin relaxation NMR spectroscopy. *Methods* **139**, 76-84 (2018).

53. Butterwick, J.A., Patrick Loria, J., Astrof, N.S., Kroenke, C.D., Cole, R., Rance, M. & Palmer, A.G. Multiple time scale backbone dynamics of homologous thermophilic and mesophilic ribonuclease HI enzymes. *J. Mol. Biol.* **339**, 855-871 (2004).

54. Butterwick, J.A. & Palmer, A.G. An inserted gly residue fine tunes dynamics between mesophilic and thermophilic ribonucleases H. *Protein Sci.* **15**, 2697-707 (2006).

55. Stafford, K.A., Robustelli, P. & Palmer, A.G. Thermal adaptation of conformational dynamics in ribonuclease H. *PLoS Comput. Biol.* **9**, e1003218 (2013).

56. Stafford, K.A., Trbovic, N., Butterwick, J.A., Abel, R., Friesner, R.A. & Palmer, A.G. Conformational preferences underlying reduced activity of a thermophilic ribonuclease H. *J. Mol. Biol.* **427**, 853-866 (2015).

57. Bleijlevens, B., Shivarattan, T., Flashman, E., Yang, Y., Simpson, P.J., Koivisto, P., Sedgwick, B., Schofield, C.J. & Matthews, S.J. Dynamic states of the DNA repair enzyme AlkB regulate product release. *EMBO Reports* **9**, 872–877 (2008).

58. Bleijlevens, B., Shivarattan, T., van den Boom, K.S., de Haan, A., van der Zwan, G., Simpson, P.J. & Matthews, S.J. Changes in protein dynamics of the DNA repair dioxygenase AlkB upon binding of Fe^{2+} and 2-oxoglutarate. *Biochemistry* **51**, 3334-3341 (2012).

Table 1. Apparent activation energies

Residue	Activation Energy ($E_{app}^{\dagger}$, kJ/mol)
Val 98 γ1	45.4 ± 1.6
Val 101 γ1	23.7 ± 1.9
Leu103 δ1	21.4 ± 3.0

Estimated apparent activation energies ($E_{app}^{\dagger}$) as determined from the temperature dependence of ΔR_{ex} vs 1/T using Eq. 6, as shown in Figure 4d.

Figures

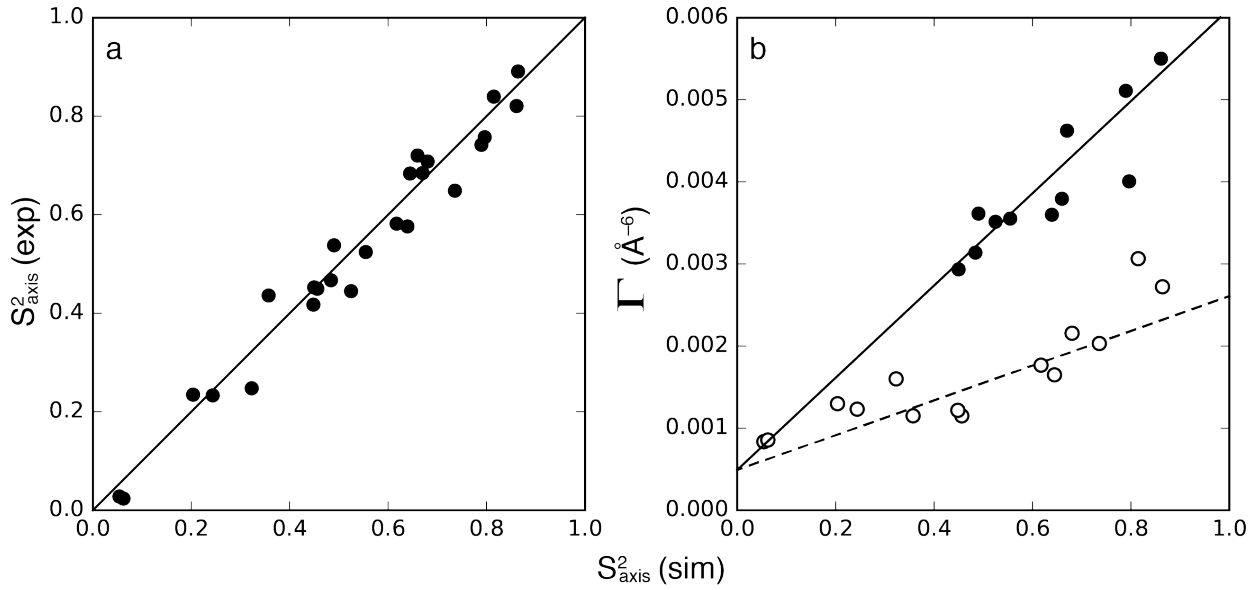

Figure 1. (a) Comparison between experimental and MD simulated values of S^2_{axis} for 25 methyl groups for which the absolute deviation is < 0.1. (b) Values of Γ determined from MD simulations are plotted versus the simulated values of S^2_{axis} for the same methyl groups shown in (a). Two lines are plotted for the (solid symbols, solid line) subset of data with maximum slope and (empty symbols, dashed line) subset of data with minimum slope. The intercepts of the plotted lines are set equal to the fitted line for dashed line.

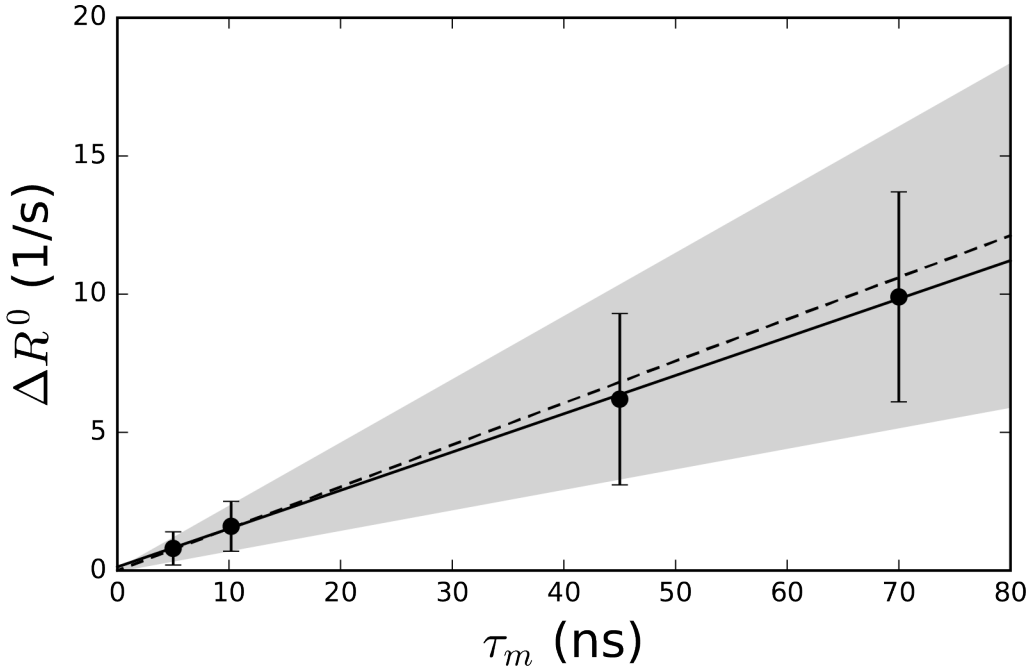

Figure 2. Experimental and predicted values of ΔR^0 versus τ_c. (solid, circles) Experimental values of ΔR_{MQ} measured for protein L (5° and 25° C) and malate synthase G (20° and 37° C), assuming minimal contributions from exchange [14]. (dashed) Average values calculated from the values of Γ determined from MD simulations of RNase H. The shaded region shows ± standard deviation of the calculations. Calculations were performed for the 25 methyl groups used in Figure 1.

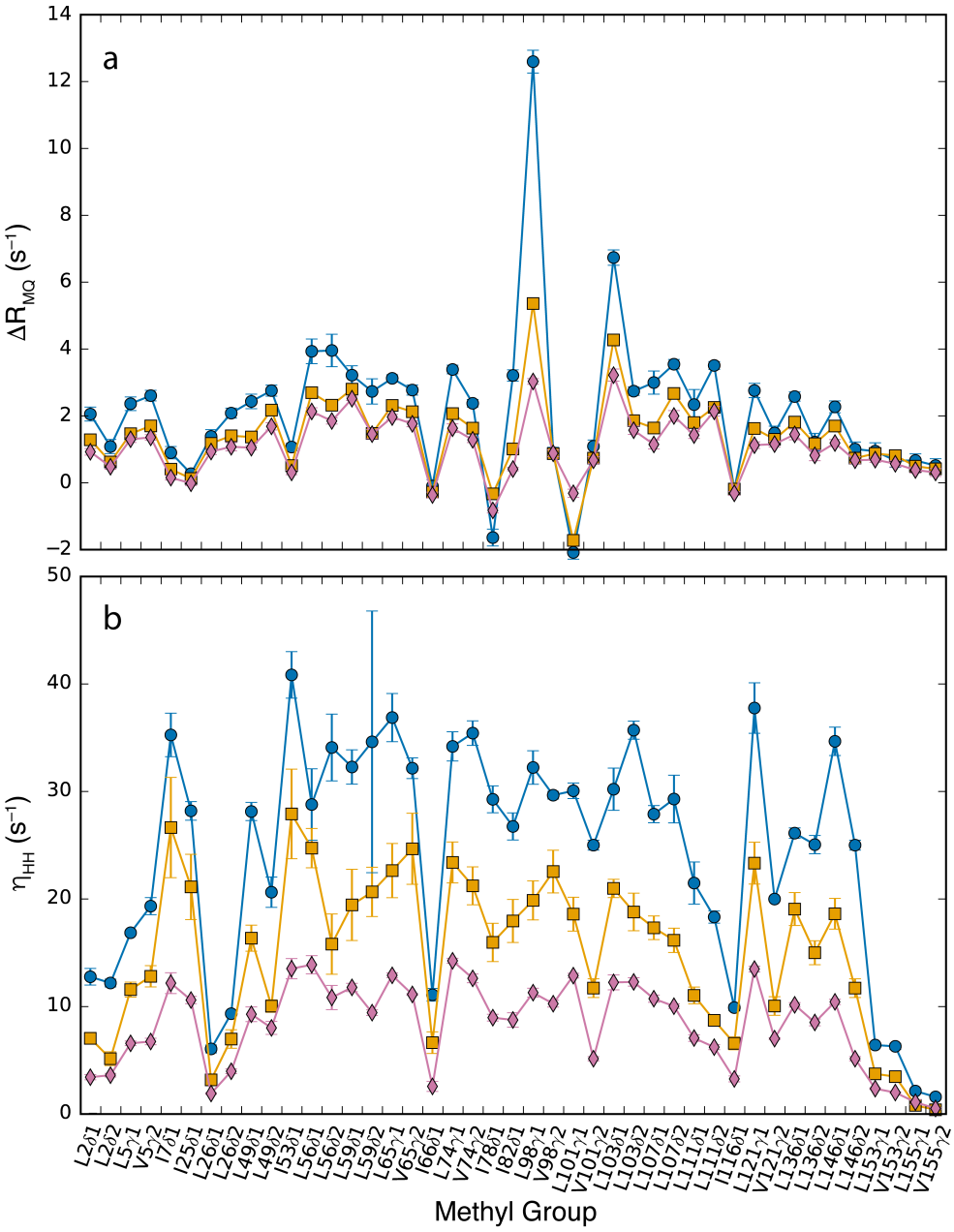

Figure 3. (a) Differential relaxation rate of zero- and double-quantum coherence (ΔR_{MQ}) and (b) ^{1}H-^{1}H dipole-dipole cross-correlated relaxation rate constant (η_{HH}) for Ile, Leu, and Val residues of RNase H measured at (blue, circles) 283, (orange, squares) 300, and (reddish-purple, diamonds) 310 K, respectively.

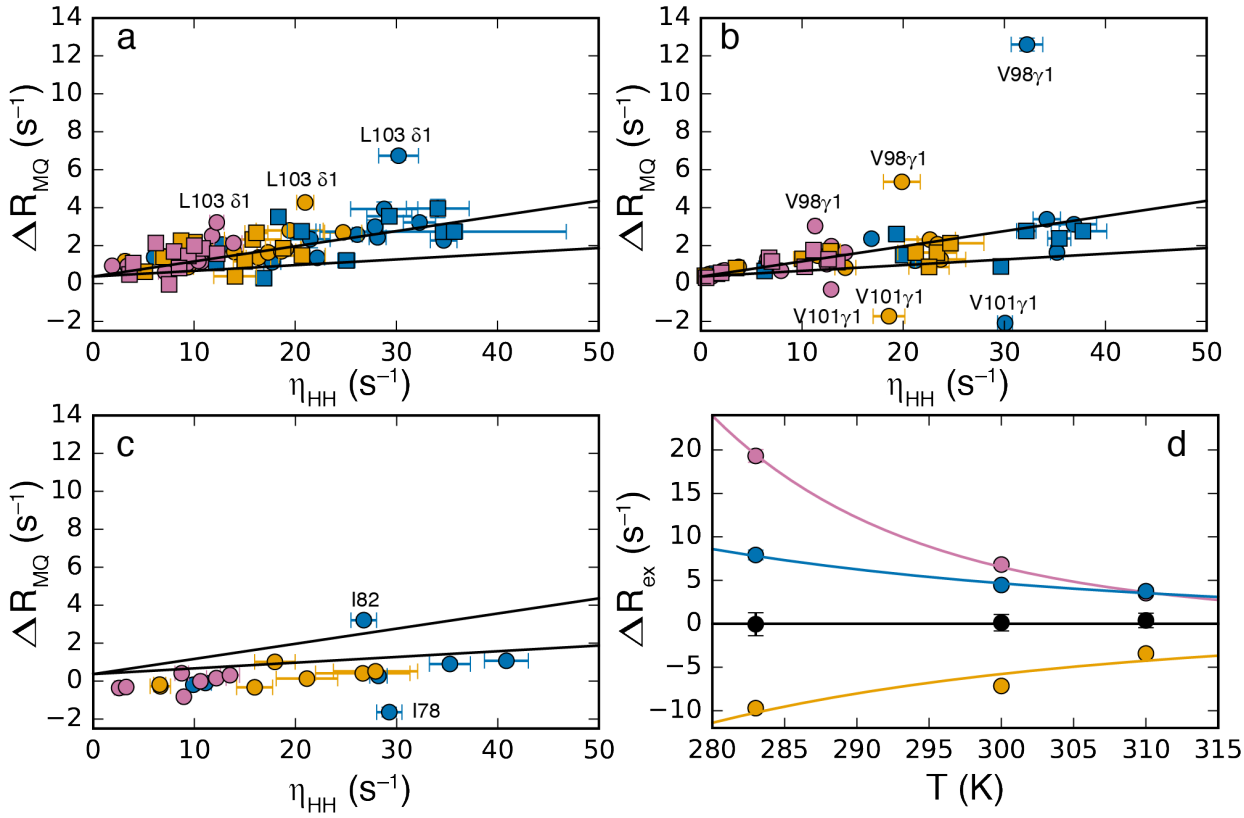

Figure 4. Values of ΔR_{MQ} vs. η_{HH} are shown for RNase H (a) Leu δ1 (circles) and δ2 (squares), (b) Val γ1 (circles) and γ2 (squares), and (c) Ile δ1 methyl groups at (blue) 283 K, (orange) 300 K, and (reddish-purple) 310 K. The solid line is the mean result calculated as $\kappa_{ILV}\,\eta_{HH}$. The shaded region shows ± the standard deviation in the mean of the calculation. (d) Arrhenius plot for (reddish-purple) Val 98 γ1, (orange) Val 101 γ1, (blue) Leu 103 δ1, and (black, circles) mean of all other Leu and Val residues. Solid lines for Val 98 γ1, Val 101 γ1, and Leu 103 δ1 show best single-exponential fits to the data to obtain $E_{app}^{\dagger}$, given in Table 1.

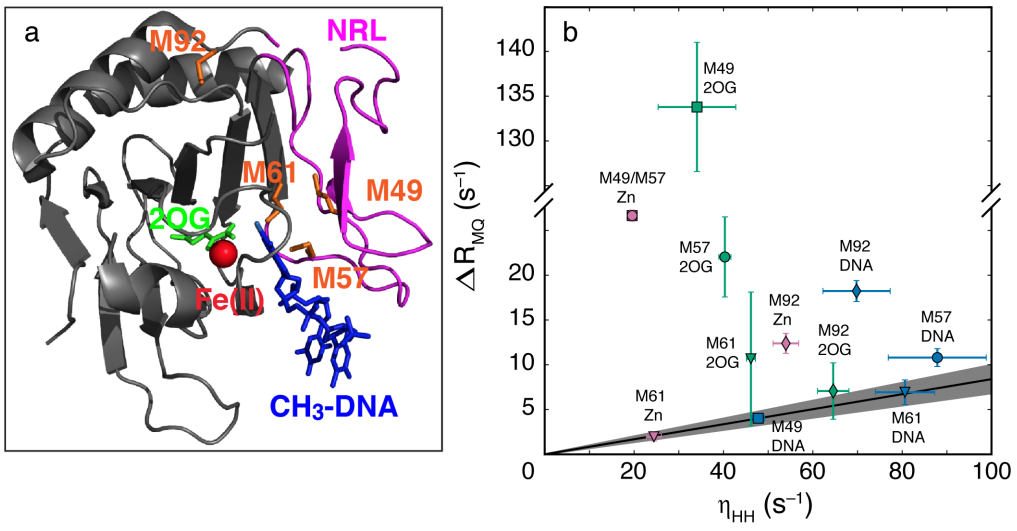

Figure 5. Chemical exchange in AlkB. (a) Ribbon diagram showing the crystal structure of AlkB-N11 with bound Fe(II) (red), 2-oxoglutarate (2OG, green), and methylated DNA substrate (blue) drawn from PDB code 2FD8. The Fe(II)/2OG core and nucleotide recognition lid are colored grey and magenta, respectively, and the residues used as spectroscopic probes are shown in orange stick representation. (b) Values of ΔR_{MQ} vs. η_{HH} are shown for AlkB. M49 (squares), M57 (circles), M61 (triangles) and M92 (diamonds) are shown for AlkB in successive complex with Zn^{2+} (reddish-purple), Zn^{2+}/2OG (green), and Zn^{2+}/2OG/DNA substrate (blue). The solid line is the mean empirical result calculated as $\kappa_{Met}\eta_{HH}$ (see main text). The shaded region shows ± the standard deviation of the calculations. M49 and M57 are degenerate in the Zn^{2+} complex.